

Synthesis of silver nanoparticles and antimony oxide nanocrystals by pulsed laser ablation in liquid media

M.I. Mendivil · B. Krishnan · F.A. Sanchez ·
S. Martinez · J.A. Aguilar-Martinez · G.A. Castillo ·
D.I. Garcia-Gutierrez · S. Shaji

Received: 23 August 2011 / Accepted: 3 August 2012 / Published online: 25 August 2012
© Springer-Verlag 2012

Abstract Pulsed laser ablation in liquid media (PLALM) is a prominent technique for the controlled fabrication of nanomaterials via rapid reactive quenching of ablated species at the interface between the plasma and liquid. Results on nanoparticles and nanocrystals formed by PLALM of silver (Ag) and antimony (Sb) solid targets in different liquid environments (Sodium Dodecyl Sulfate, distilled water) are presented. These experiments were done by irradiating solid targets of Ag and Sb with a nanosecond pulsed Nd:YAG laser output of wavelength 532 nm. Nanoparticles of silver and nanocrystals of antimony oxide (Sb_2O_3) obtained were characterized using UV-Vis spectrometry, Scanning Electron Microscopy (SEM), transmission electron microscopy (TEM), X-ray Energy Dispersion Analysis (EDAX) and X-ray diffractometry (XRD). The morphology of nanomaterials formed is studied as a function of surfactant environment. The silver nanoparticles obtained were spherical of size in the order of 10–35 nm in solution of SDS having different concentrations. In case of the Sb target, ablation was performed in two different molarities of SDS solution and distilled water. Nanocrystals of Sb_2O_3 in powder form having cubic and orthorhombic phases were formed in SDS

solution and as fibers of nanocrystals of cubic Sb_2O_3 in distilled water.

1 Introduction

Pulsed laser ablation in liquid media (PLALM) is a remarkable, unique process for the fabrication of nanomaterials using the physical laser ablation phenomenon and subsequent chemical reactions. This process leads to the release of nanoclusters to the surfactant environment and the formation of colloidal nanoparticle solution. This method is widely used in production of various kinds of nanoparticle, like noble metals, alloys, oxides, and semiconductors. Formation of metal nanoparticles by PLALM has been achieved by various groups. Mafune et al. [1–3] obtained gold nanoparticles of 1–5 nm diameter by PLALM of gold metal plate in aqueous solution of SDS using a Nd:YAG laser operated at wavelength 1064 nm and 532 nm. Kabashin group [4] reported the size control and stability of gold nanoparticles produced during femtosecond PLALM in aqueous cyclodextrins. Simakin et al. [5] reviewed the results on nanoparticle formation of silver (Ag), gold (Au) and titanium (Ti) solid targets by pulsed laser ablation in liquid media (H_2O , $\text{C}_2\text{H}_4\text{Cl}_2$, ethanol etc.). In this review, they reported the formation of Au–Ag alloy by laser irradiation of colloidal nanoparticles and results of their studies on influence of the nature of liquids and laser parameters on the properties of the nanoparticles. The stability, size, and optical properties of silver nanoparticles prepared by PLALM using 1064 nm Nd:YAG laser output in acetone, water, and ethanol were studied [6], which included discussions on nucleation, growth, and aggregation mechanisms which were related to the polarity of the surfactant solutions where highly polar

M.I. Mendivil · B. Krishnan · F.A. Sanchez · S. Martinez ·
J.A. Aguilar-Martinez · G.A. Castillo · D.I. Garcia-Gutierrez ·
S. Shaji (✉)
Facultad de Ingeniería Mecánica y Eléctrica, Universidad
Autónoma de Nuevo León, San Nicolás de los Garza, Nuevo
León, Mexico, 66450
e-mail: sshajis@yahoo.com

B. Krishnan · D.I. Garcia-Gutierrez · S. Shaji
Universidad Autónoma de Nuevo León, CIIDIT, Apodaca, Nuevo
León, Mexico

J.A. Aguilar-Martinez
CIMAV Monterrey, PIIT, Apodaca, Nuevo León, Mexico

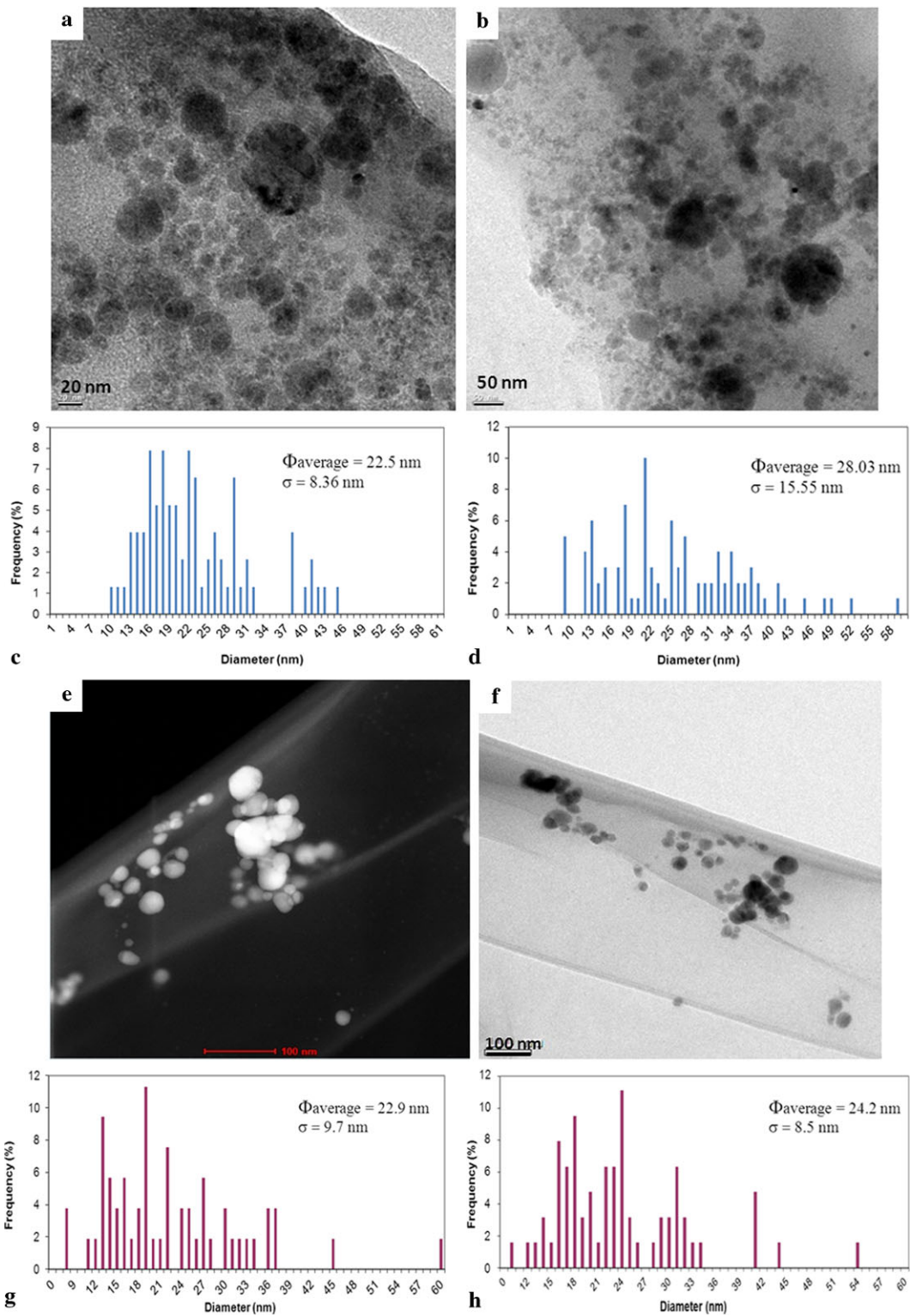
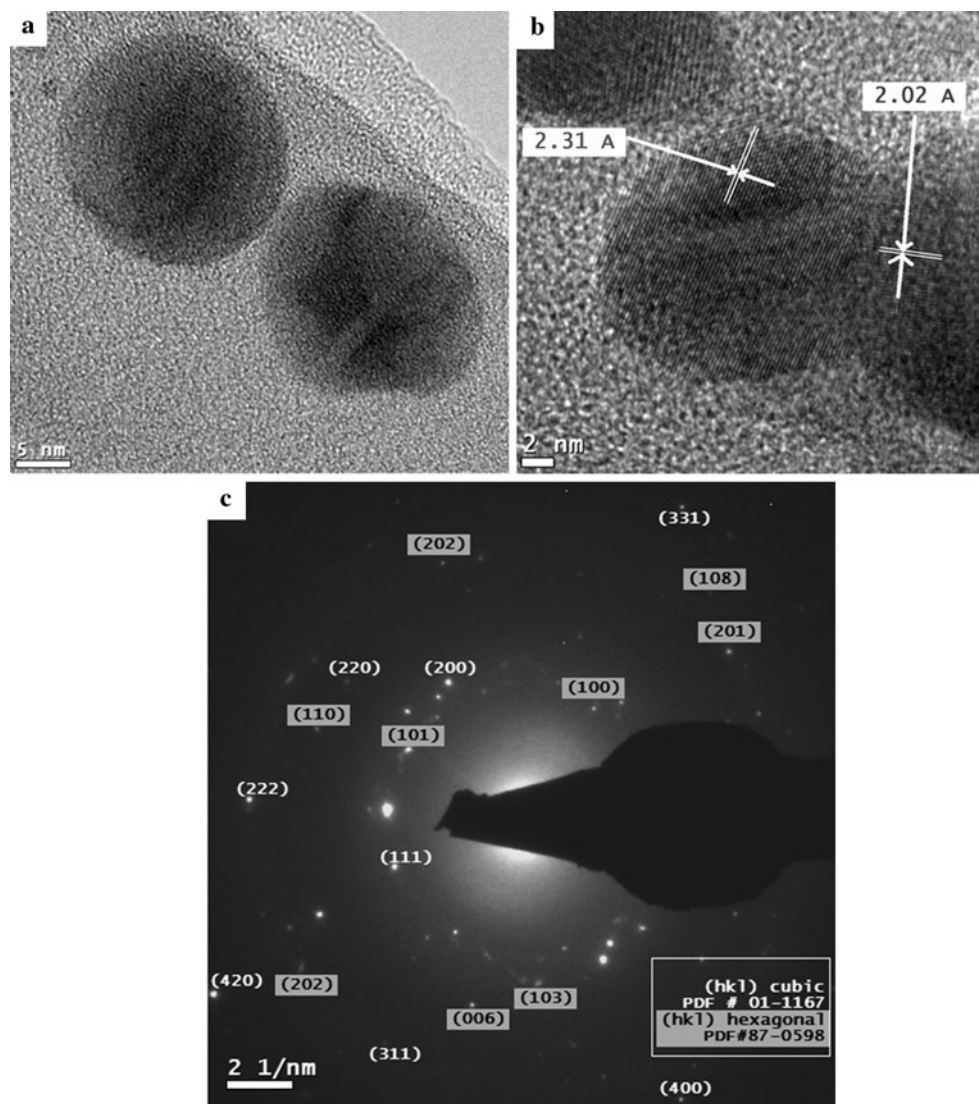


Fig. 1 TEM images and the corresponding size distributions of silver nanoparticles obtained by PLALM (**a–d**) in 0.05 M SDS solution (**e–h**) 0.01 M SDS solution. Images (**a, b**) were collected from two regions

of the same sample obtained in 0.05 M and (**e, f**) were images from two regions of the sample obtained in 0.01 M

Fig. 2 HRTEM images of silver nanoparticles obtained in (a, b) 0.01 M SDS solution and (c) the corresponding electron diffraction pattern. The interplanar distances observed in HRTEM are highlighted in (b) and the reflections from various planes of cubic and hexagonal phases of silver are included in (c)



molecules can strongly provide a surrounding electrical double layer to prevent growth, aggregation, and precipitation. Silver nanoparticles were produced by ablation of Ag target in water using 532 nm pulsed YAG output and obtained nanoparticles of 2–5 nm in size. Possible particle formation mechanisms and the influence of parameters like beam spot size, laser power and ablation time were described [7]. Silicon nanoparticles were synthesized by femtosecond laser ablation of silicon target in water and their optical properties were discussed [8]. Palladium nanoparticles were produced by PLALM in water and aqueous solutions of SDS and well characterized [9]. Oxide nanoparticles were obtained in a single step, a fast and easy process by PLALM of metal targets in water/aqueous solutions/alcohols etc. ZnO nanoparticles were obtained by ablation of a zinc metal plate in cationic, anionic amphoteric and non-ionic solutions by Usui et al. [10]. Metal oxide/sulfide hollow nanoparticles were fabricated by ablation of metal targets (Zn, Pb, Mg, Cu,

Co, Fe, and Ti) in selected liquids (water/ethanol, n-hexane, β -mercaptoethanol etc.) [11]. Lin et al. [12] synthesized and characterized ZnO and Zn(OH)₂ composite nanoparticles by ablation of Zn target in water using 1064 nm and 532 nm output from a YAG laser.

Oxides of Antimony (OA) have been widely used in chemical, sensing, and semiconducting industries [13, 14]. OA nanoparticles can be synthesized via several methods [15, 16]. However, no reports on synthesis of OA by PLALM have been found so far. In the present work the synthesis of Ag nanoparticles and antimony oxide nanocrystals by PLALM is reported.

2 Experimental

The experimental setup was similar to the reported ones [1–3]. We used the second harmonic output (532 nm) from

Table 1 The crystalline planes observed, corresponding interplanar distances in the standard (JCPDS data) and the values obtained from electron diffraction for silver nanoparticles

| Crystalline planes observed | Interplanar distances from JCPDS data (in Å units) | | Interplanar distances measured from electron diffraction (in Å units) |
|-----------------------------|--|----------------------|---|
| | Face centered cubic (#01-1167) | Hexagonal (#87-0598) | |
| (200) | 2.044 | | 2.066 |
| (100) | | 2.5 | 2.483 |
| (101) | | 2.425 | 2.430 |
| (111) | 2.36 | | 2.367 |
| (103) | | 1.999 | 1.988 |
| (006) | | 1.66 | 1.692 |
| (220) | 1.45 | | 1.459 |
| (110) | | 1.44 | 1.444 |
| (201) | | 1.2402 | 1.238 |
| (202) | | 1.21 | 1.219 |
| (311) | 1.23 | | 1.239 |
| (222) | 1.18 | | 1.191 |
| (108) | | 1.11 | 1.12 |
| (400) | 1.02 | | 1.044 |
| (331) | 0.94 | | 0.95 |
| (420) | 0.92 | | 0.919 |

a pulsed Nd:YAG laser (energy 140 mJ/pulse, repetition frequency 10 Hz, pulse width 5 ns). Highly pure (99.99 % purity) silver foil and antimony rod (99.99 % purity) were used as targets of ablation. The ablation of silver in various concentrations of SDS solutions (1 M–0.001 M) was carried out. Silver foil was kept in 10 ml solution of SDS in a small beaker and the laser beam was focused using a convex lens of 20 cm focal length. The ablation time was 10 minutes. The clear solution of SDS was turned to colored one when the silver nanoparticles were formed in the colloidal solution. Ablation of antimony was carried out in two molarities of SDS (1 M and 0.1 M) and in distilled water.

The silver nanoparticles and antimony oxide nanocrystals obtained were characterized using various techniques. The optical absorption spectra of colloidal silver nanoparticles in SDS solution were measured using a Perkin-Elmer UV-Vis- spectrophotometer. Morphological studies were done using Scanning Electron Microscopy (SEM-FEI Nova NanoSEM 200) and Transmission Electron Microscopy (TEM-FEI Titan G² 80-300) and elemental analysis using an Energy Dispersive X-ray Analyzer (EDAX) associated with the SEM and TEM. The samples for TEM analysis were prepared by depositing a drop of the solution containing silver nanoparticles onto carbon coated copper grids and dried completely at room temperature. Structural characterization was done using electron diffraction and X-ray diffraction (XRD) patterns. The XRD pattern of the antimony oxide nanocrystals were recorded using a Panalytical Empyrean diffractometer employing Cu K α 1 radiation

($\lambda = 1.54056 \text{ \AA}$) at normal mode. The scan range was 10–70°.

3 Results and discussion

3.1 Silver nanoparticles

3.1.1 Transmission Electron Microscopy (TEM) and Electron Diffraction

The morphology and size distributions of silver nanoparticles are analyzed using TEM and High Resolution TEM (HRTEM). The TEM images of silver nanoparticles obtained in 0.05 M SDS solution and their size distributions are shown in Fig. 1(a–d). Figure 1(a) and (b) are the images from two different regions of the same sample. The average size (Φ average) of the silver nanoparticles obtained is 22 to 28 nm as indicated in Fig. 1(c, d). Figure 1(e–h) shows the TEM images and corresponding size distributions of Ag nanoparticles obtained in 0.01 M SDS solution at two different locations of the same sample. In this case, the average size (Φ average) of the silver nanoparticles obtained is 23 to 24 nm. We observed agglomeration of nanoparticles in all the SDS concentrations. An EDAX analysis confirmed metallic silver. Electron diffraction pattern was recorded to obtain the crystalline structure of these nanoparticles. Figure 2(a) and (b) show the HRTEM images of silver nanoparticles and Fig. 2(c), the electron diffraction pattern for Ag nanoparticles obtained in 0.01 M SDS. By comparing with

the standard JCPDS data for face centered cubic (FCC) (#01-1167) and hexagonal (#87-0598) patterns of silver, it was observed that the silver nanoparticles were of cubic and hexagonal phases and the reflections from these planes were labeled in Fig. 2(c). The interplanar distances identified in HRTEM image for cubic structure with 2.31 Å and 2.02 Å are indicated in Fig. 2(b). Table 1 shows the reflection planes

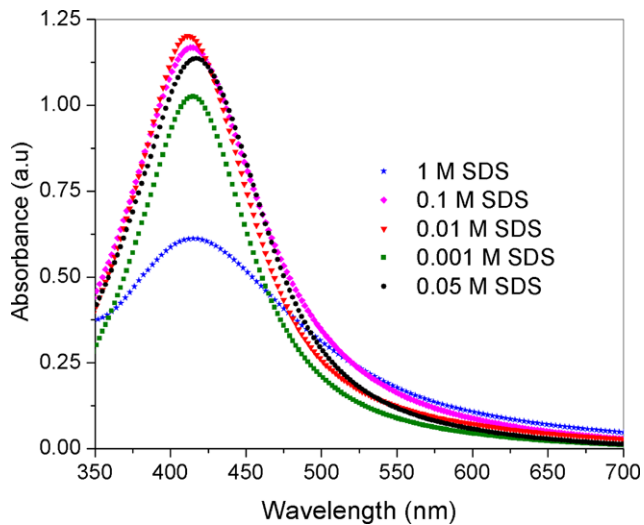
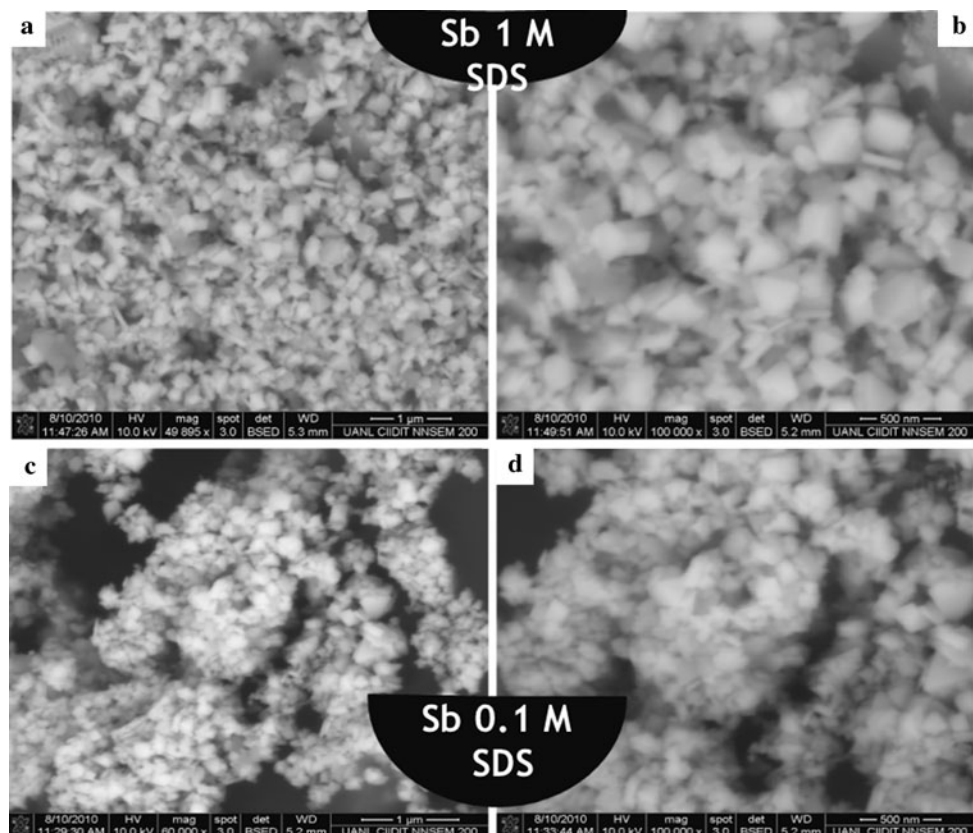


Fig. 3 Optical absorption spectra of silver nanoparticles produced by PLALM in different molarities of SDS solution

Fig. 4 SEM images of antimony oxide nanocrystals obtained by PLALM of antimony in (a) 1 M SDS solution and (b) a higher magnification of the same (c) 0.1 M SDS solution and (d) a higher magnification of the same

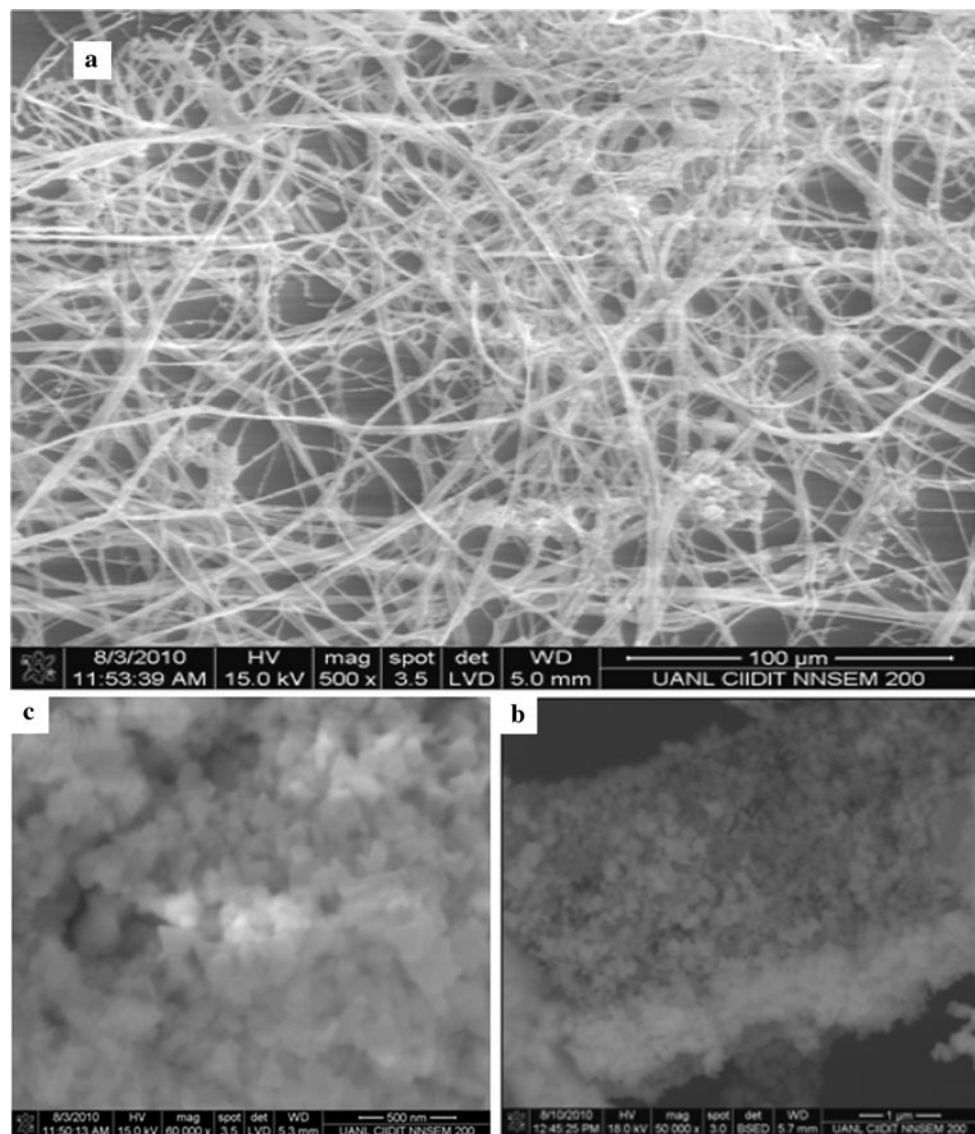


identified and the interplanar distances measured from the electron diffraction pattern for both cubic and hexagonal phases of silver nanoparticles. Interplanar distances from the standard JCPDS data for silver are also included for comparison. Similar crystalline structure was detected for silver nanoparticles synthesized in other molarities of SDS solution.

3.1.2 Optical absorption spectra

The optical properties of silver nanoparticles were studied by optical absorption spectral measurements in the visible region for colloidal solutions of silver nanoparticles. The absorption spectra of silver nanoparticles obtained by pulsed laser ablation of silver target in various molarities of aqueous solution of SDS are shown in Fig. 3. The plasmon-resonance peaks of silver nanoparticles were around 412–417 nm. In general, silver nanoparticles show a plasmon resonance around 400 nm [5, 6] and also the position is related to the size and shape of the nanoparticles. The broadening of the absorption peaks depends on the size distribution and agglomeration of the nanoparticles. From the absorption spectra, the full width at half maximum (FWHM) for the peaks calculated was nearly 100 nm for all the samples. We could not observe noticeable changes in the plasmon-resonance peak positions for various concentrations of SDS.

Fig. 5 (a) SEM image of antimony oxide nanocrystals obtained by PLALM of antimony in distilled water, (b, c) images at higher magnification of one of the fibers in (a)



This may be due to the wide particle size distributions and agglomerations of the Ag nanoparticles as observed in the TEM analysis (Fig. 1(a–h)).

3.2 Antimony oxide nanocrystals

PLALM of Sb target in aqueous solutions of SDS and distilled water resulted in formation of antimony oxide nanocrystals.

3.2.1 SEM with EDAX

In SDS solution, the nanocrystals formed were of powder form. The SEM images of the antimony oxide nanocrystals obtained in 1 M SDS solution are shown in Fig. 4(a) and that of higher magnification in Fig. 4(b). Figures 4(c) and (d) depict SEM images of the nanocrystals obtained in

0.1 M SDS solution under lower and higher magnifications, respectively. It shows the presence of nanocrystals of antimony oxide of varying sizes. No changes in the morphology were observed for these two concentrations of SDS solution. Antimony oxide nanocrystals formed by ablation of antimony in distilled water were having a fiber like structure as shown in Fig. 5(a). Higher magnification images of one of these fibers are shown in Fig. 5(b) and (c). It is observed that these fibers were composed of numerous nanocrystals of antimony oxide. An EDAX analysis was performed, showing the presence of antimony and oxygen. The formation of antimony oxide by ablation of antimony target in SDS solution and water could be explained using the method of reactive laser ablation in liquid as described by Zeng et al. [17]. The antimony species ablated from the solid target reacted with the surrounding liquid medium, in these cases SDS solution and water forming antimony oxide. The oxygen for

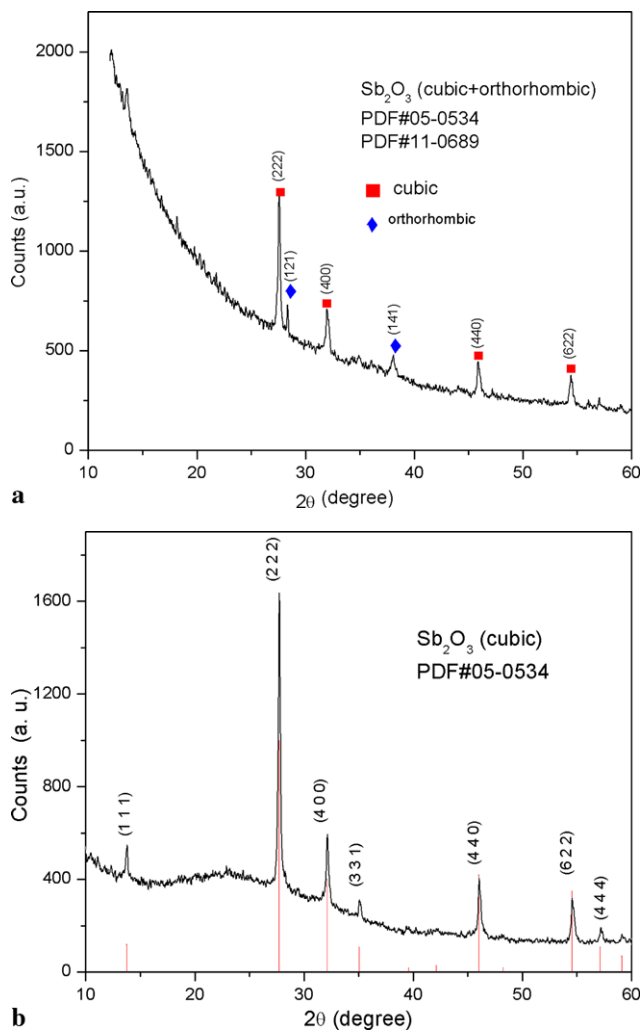


Fig. 6 XRD patterns of antimony oxide (Sb_2O_3) obtained by PLALM (a) in 1 M SDS solution and (b) distilled water. The standard JCPDS data for cubic (PDF#05-0534) and orthorhombic (PDF#11-0689) structures of Sb_2O_3 are also included

the oxide formation is obtained from water present in these cases. The nature of the surfactant solution resulted in different plasma states in the ablation process, leading to the formation of different phases and morphologies for antimony oxide.

3.2.2 XRD

The X-ray diffraction patterns obtained for antimony oxide are given in Fig. 6(a) and (b). The powder obtained by PLALM of antimony in SDS solution showed the presence of antimony oxide (Sb_2O_3) having cubic and orthorhombic structures (Fig. 6(a)), a mixed phase. The standard peak positions corresponding to reflections from various planes for cubic (PDF#05-0534) and orthorhombic (PDF#11-0689) structures were in good agreement with the diffraction pattern obtained. While the pattern for the antimony oxide

nanocrystals formed (fiber like structure) by ablation of antimony in distilled water showed the presence of cubic structure (Fig. 6(b)), single phase. All the peaks observed in this case match with the reflections from the standard pattern (PDF#05-0534) corresponding to cubic structure of antimony oxide (Sb_2O_3). The average crystallite size estimated using the Scherrer formula was of 35 nm. The interesting result was the formation of antimony oxide nanocrystals having different crystalline structures in different surfactant solutions.

4 Conclusions

We have obtained silver nanoparticles spherical in shape by pulsed laser ablation of silver target in various concentrations of SDS solutions. These nanoparticles were having an average size of 24 nm having cubic and hexagonal crystalline phases. PLALM of antimony in an aqueous solution of SDS produced nanocrystals of Sb_2O_3 as powders. These nanocrystals were composed of two phases of antimony oxide—cubic and orthorhombic. PLALM of Sb in distilled water formed Sb_2O_3 in fiber forms, which were composed of nanocrystals of Sb_2O_3 of cubic phase only. The morphology of Sb_2O_3 was affected by the surfactant; resulting in the formation of nanocrystals of Sb_2O_3 as powders and fibers, in SDS and distilled water, respectively. This is the first report of synthesis of Sb_2O_3 by PLALM and also the fabrication of different crystalline phases of an oxide nanocrystal by varying the surfactant media.

Acknowledgements The authors are thankful to PAICYT-UANL, PROMEP, and SEP-CONACYT-Mexico (project 106955) for the financial assistance. One of the authors, M.I. Mendivil is grateful to CONACYT-Mexico for providing a research Fellowship.

References

1. F. Mafune, J. Kohno, Y. Takeda, *J. Phys. Chem. B* **105**, 5114 (2001)
2. F. Mafune, J. Kohno, Y. Takeda, *J. Phys. Chem. B* **107**, 4218 (2003)
3. F. Mafune, J. Kohno, Y. Takeda, *J. Phys. Chem. B* **106**, 7575 (2002)
4. A.V. Kabashin, M. Meunier, C. Kingston, *J. Phys. Chem. B* **107**, 4527 (2003)
5. A.V. Simakin, V.V. Voronov, N.A. Kirichenko, G.A. Shafeev, *Appl. Phys. A* **79**, 1127 (2004)
6. R.M. Tilaki, A.I. Zad, S.M. Mahdavi, *Appl. Phys. A* **84**, 215 (2006)
7. A. Pyatenko, K. Shimokawa, M. Yamaguchi, O. Nishimura, M. Suzuki, *Appl. Phys. A* **79**, 803 (2004)
8. R. Intartaglia, K. Bagga, F. Brandi, G. Das, A. Genovese, E. Di Fabrizio, A. Diaspro, *J. Phys. Chem. C* **115**, 5102 (2011)
9. G. Cristoforetti, E. Pitzalis, R. Spiniello, R. Ishak, M. Muniz-Miranda, *J. Phys. Chem. C* **115**, 5073 (2011)

10. H. Usui, Y. Shimizu, T. Sasaki, N. Koshizaki, *J. Phys. Chem. B* **109**, 120 (2005)
11. K.Y. Niu, J. Yang, S.A. Kulinich, J. Sun, X.W. Du, *Langmuir* **26**, 16652 (2010)
12. B.C. Lin, P. Shen, S.Y. Chen, *J. Phys. Chem. C* **115**, 5003 (2011)
13. C.S. Xie, J.H. Hu, R. Wu, H. Xia, *Nanostruct. Mater.* **11**, 1061 (1999)
14. Z.L. Zhang, L. Guo, W.D. Wang, *J. Matter. Res.* **16**, 803 (2001)
15. N.K. Sahoo, K.V.S.R. Apparao, *Appl. Phys. A* **63**, 195 (1998)
16. S.M. Mostashari, S. Baie, *J. Therm. Anal. Calorim.* **94**, 97 (2008)
17. H. Zeng, X. Du, S.C. Singh, S.A. Kulinich, S. Yang, J. He, W. Cai, *Adv. Funct. Mater.* **22**, 1333 (2012)